Proceedings of ASME Turbo Expo 2011
GT2011
June 6-10, 2011, Vancouver, British Columbia, Canada

GT2011-46427

INVESTIGATION OF THE EFFECT OF ROTATION ON THE FLOW IN A TWO-PASS COOLING SYSTEM WITH SMOOTH AND RIBBED WALLS USING PIV

Michael Schroll **Lena Lange** **Martin Elfert**

DLR, German Aerospace Center, Institute of Propulsion Technology, D-51170 Cologne, Germany

ABSTRACT

A rotating cooling system with a 180 deg turn is investigated experimentally using the 2C PIV technique to measure the flow inside. This cooling configuration consists of two ducts of arbitrary cross-sections representing a two-pass front part of an idealized but nevertheless engine relevant turbine blade cooling design. The system has been investigated with ribbed walls in both passages for cooling enhancement as well as with smooth walls as a reference version in order to identify the effects induced by ribs. The rib orientation on the walls is 45 deg. With a rib height of 0.1 of hydraulic duct diameter and a pitch of 10 times rib height, a representative well-established rib lay-out was selected.

This paper presents measurements of the axial flow during rotation of this two-pass system for rotation numbers up to 0.1. Together with previously obtained stationary results [1], this data completes the investigation of the secondary flow field with rotational results acquired with a two-component PIV measuring technique with improved sequencer technique [2].

The Two-Pass Cooling System was analyzed on the rotating test rig using two-component Particle Image Velocimetry (2C PIV) a non-intrusive optical planar measurement technique. PIV is capable of obtaining complete flow maps of the instantaneous as well as averaged flow field even at high turbulence levels, which are typical for the narrow serpentine-shaped ribbed cooling systems. An in-house developed synchronization device enables very accurate control of the laser flashes and image acquisition with regard to the angular position of the measurement plane (light sheet) and thereby very accurately stabilizes the position of the channel within the image during PIV recording which then leads to very accurate mean velocities.

The presented investigations were conducted in stationary and rotating mode. The results demonstrate the combined interaction of different vortices induced by several effects such as the inclination of ribs, Coriolis forces due to rotation and inertial forces within the bend. Additionally, a flow separation was observed at the divider wall downstream of the bend (in the second pass) that has a strong impact on the flow field depending on the rotational speed. The axial flow maps presented in this paper in combination with the secondary flow maps published previously are of sufficient high quality and spatial resolution to serve as a benchmark test case for the validation of flow solvers. The turbulent channel flow was investigated at a Reynolds number of 50,000 and at rotation numbers of 0.0 and 0.1.

KEYWORDS: turbine blade, blade cooling, rotational effects, Coriolis force, Dean vortex, U-turn, two-pass cooling system, ribs, flow measurements, particle image velocimetry, PIV, flow field diagnostics, CFD validation

NOMENCLATURE

α	deg	rib orientation angle
b	mm	bend height, gap
d	mm	reference length, bottom side 1st pass
$d_{h.1}$, $d_{h.2}$	mm	hydraulic diameter, 1st and 2nd pass
e_1, e_2	mm	rib height, 1st and 2nd pass
E	mm	eccentricity at duct entry
p	mm	rib spacing
Re	-	Reynolds number ($\rho\ v_0\ d_{h.2} / \mu$)
Ro	-	rotation number ($\omega\ d_{h.2} / v_0$)
v_0	m/s	fluid mean velocity in the first pass
v_x, v_y	m/s	velocitiy components by PIV
v'_x, v'_y	m/s	velocity component fluctuations by PIV
x, y, z	mm	Cartesian coordinates
z_0	mm	local duct coordinate

GREEK SYMBOLS

μ	N s/m²	dynamic viscosity
ρ	kg/m³	density
ω	1/s	angular velocity

ABBREVIATIONS

L2F	**L**aser-**2**-**F**ocus **V**elocimetry
LDA	**L**aser-**D**oppler **A**nemometry
PIV	**P**article **I**mage **V**elocimetry

INTRODUCTION

The main interest in turbine blade cooling research is focused on heat transfer and pressure loss that are both mainly affected by the cooling flow inside. The flow in a rotating channel is significantly different from the flow in a non-rotating channel. The rotation changes velocity and turbulence distribution. Lezius and Johnston analyzed flow instability in a straight rectangular channel with smooth walls caused by rotation [3]. They reported that rotation increases flow velocity and turbulence near the trailing wall and reduces the turbulent fluctuations significantly near the stable leading wall. In previous investigations by Elfert et al. the velocity and turbulence distributions were measured via L2F in a rotating circular pipe with radial out- and inward directed flow [4],[5]. Rotation was found to shift the bulk flow towards the trailing wall and reduces velocity and increases turbulence at the leading wall. Rathjen measured heat transfer and fluid flow in a 2-pass-system [6]. Tse and McGrath used LDA to measure rotating flow in a two-pass channel with smooth and ribbed walls [7]. Tse and Steuber investigated the mean flow characteristics using LDA in the first and second passage with 45° ribs of semi-circular cross section during rotation [8]. Cheah et al. used the LDA to measure the velocity and turbulence quantities in a rotating two-pass channel [9]. Bons and Kerrebrock measured the internal flow in a straight smooth-wall channel with PIV with and without buoyancy [10]. Both Schabacker et al. as well as Chanteloup also used PIV to measure the flows in two-pass square ducts with 45° inclined ribs, although non-rotating [11],[12]. Son et al. measured the flow using PIV in two-pass channels with smooth and 90° ribbed walls [13]. Liou and Chen measured the developing flow in a two-pass smooth duct with LDA [14]. Liou et al. measured the fluid flow in a rotating two-pass duct with 90° ribs [15] and they performed LDV measurements for detached 90° ribs [16]. Liou and Dai measured pressure and flow characteristics in a rotating two-pass square duct with 45° angled ribs of square cross section using the LDA [17]. Liou et al. measured flow and pressure fields in a rotating two-pass duct with staggered 45° ribs of rounded cross section [18].

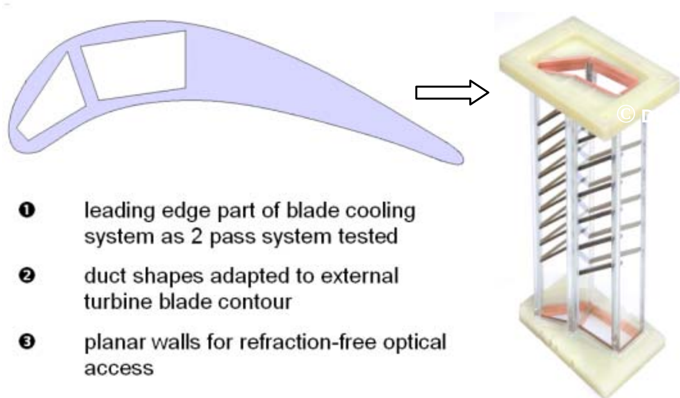

Fig. 1 Front part of an internal blade cooling system (left) and transparent model of the selected 2-pass system (right)

Elfert and Jarius used PIV to obtain flow velocity components and fluctuations in a 2-pass-cooling system with an engine-similar geometry and ribbed walls [19],[20],[1],[21]. Elfert, Voges and Klinner showed PIV measurements in a rotating two-pass system with rectangular cross-sections and wall ribs [22]. From a rotating water model, incompressible data were published by Gallo [23]. The flow measurements cited above help the understanding of the observed flow physics and can explain some heat transfer measurements obtained without the knowledge of the governing flow [24],[25],[26].

State-of-the-art serpentine-shaped multi-pass cooling systems are equipped with ribbed walls to improve heat exchange. The tested cooling configuration represents the leading edge part of a typical blade cooling design consisting of a ribbed 2-pass system with engine similar configuration and the presence of one turn, **Fig. 1**. The duct walls are planar in order to reduce optical distortion to enable the application of the PIV technique.

The experimental investigation of rotating narrow flow channels with ribbed walls is in itself a very challenging task. Also the CFD simulation task is quite ambitious as recently mentioned by Iacovides and Launder [27]. The numerical design tools used today have to be validated with experimental data to assure an accurate simulation of the complex multi-pass coolant channel flow. With this motivation the Institute of Propulsion Technology at DLR is involved in long term research programs to provide experimental data of flow for CFD validation and developing CFD codes like the DLR flow solver TRACE.

Test Rig for the Investigation of Rotating Cooling Systems

A schematic of the test rig with sketched PIV set-up is given in **Fig. 2**. Cooling air is supplied in the rig through two rotary sealing assemblies, both mounted to the double hollow shaft. The rotor speed < 1,500 rpm is controlled by a continuously adjustable hydraulic torque converter via a belt drive.

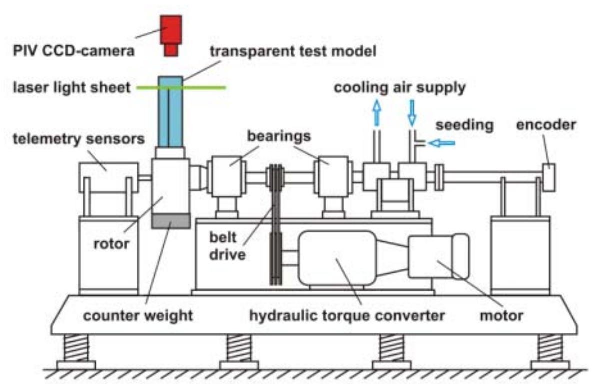

Fig. 2 Test rig for the investigation of rotating cooling systems

The rotor with the mounted test model has an outer diameter of 1 m and can be driven up to 1,500 rpm. Flow rate, spin rate and pressure level can be individually adjusted. The test model rotates perpendicular to the axis of rotation with an eccentric orientation.

Geometry of the Test Model

Fig. 1 shows a perspective view of the transparent test model. The geometry of the model including ribs is given in **Fig. 3**. The test section consists of a leading edge duct (first pass) with a trapezoidal (nearly triangular) cross-section with radially outward directed flow, a 180 deg bend and a second pass with a different trapezoidal (nearly rectangular) cross-section with radially inward directed flow. The ratio between the hydraulic diameters $d_{h.2}$ and $d_{h.1}$ of the second pass to the first pass is 1.53, the area ratio is 2.04. The length of each pass is 8.9 d with d = 25 mm (with d as length of lower side wall at first pass). The flow is not only deflected by the U-turn but also in a perpendicular xy-plane by the skewed orientation of the two ducts due to the curved shape of the turbine blade profile. The test model has a length of 10 d. The gap between tip plate and divider wall is b = 1.0 d. The web has a thickness of 0.2 d.

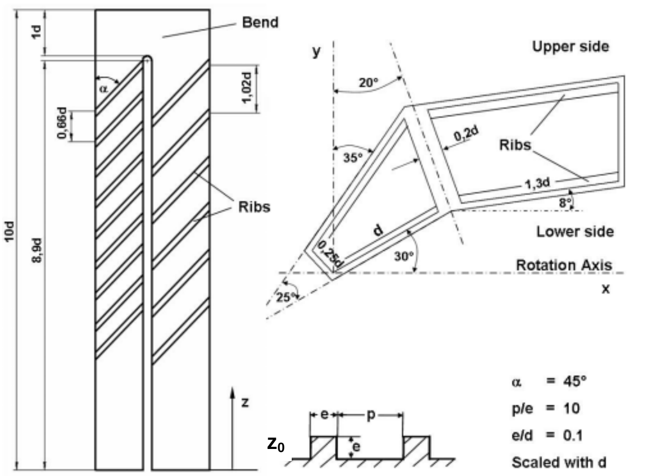

Fig. 3 Geometry of the ribbed test model (two-pass system)

The rib spacing p is 10 times rib height e. Ribs are of square cross-sections with an edge length $e_1 = 0.066$ d in the first pass and $e_2 = 0.102$ d in the second pass. The onset of ribs starts after a length of 3 d and ends, vice versa, 3 d before exit. For an appropriate numerical flow simulation, inlet casing and a part of the up-stream conduit have been included into the computational domain. The geometry of the upstream and downstream supply pipes and casings are specified by **Fig. 4**.

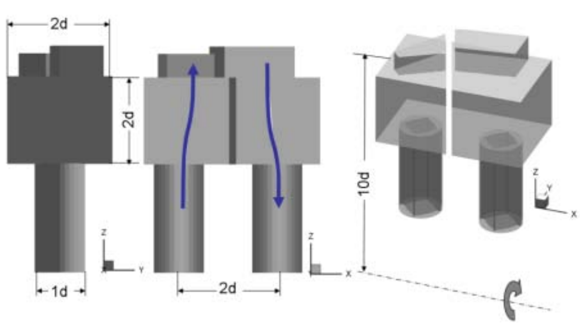

Fig. 4 System inlet, geometry of inlet and outlet plenum and upstream and downstream supply pipe

The eccentricity E at the inlet of the test model is 10 d. Flow development starts after a sharp entry into the duct. The relevant dimensionless numbers are the Reynolds number Re and the Rotation number Ro (which is the inverse of the Rossby number) defined by $d_{h.2}$ as reference diameter, v the fluid mean velocity in the second pass, ω the rotation speed, ρ and μ the mass density and the dynamic viscosity of the fluid, respectively. The Reynolds number governs the static behaviour of the flow field, while Ro is a dimensionless measure of the Coriolis effects. The presented experiments have been performed at Re = 50,000. The corresponding rotation numbers were Ro = 0.0 and 0.1. The maximum error on the Reynolds and Rotation number evaluation is better than ± 2%.

FLOW MEASURING TECHNIQUE

Particle Image Velocimetry

The unsteady flow field is measured by means of phase-locked Particle Image Velocimetry (PIV). This non-intrusive optical planar measuring technique is based on the principle of measuring the displacement of small tracer particles (aerosol, ∅ < 1 μm) within the investigated flow field. Two laser flashes, each with a flash duration of only few nanoseconds, are formed into a light sheet of about 1 mm thickness and illuminate the flow field twice within a few microseconds. The light scattered by the tracer particles is recorded via a CCD camera and enables the simultaneous acquisition of two component velocity data over the illuminated area [28],[29].

To seed the flow with tracer particles an aerosol generator is operated with a mixture of paraffin oil and ethanol. The liquid is dispersed using pressurized air at 5 bar issuing from sonic nozzles. While the ethanol evaporates, the remaining paraffin oil particles are carried with the air flow passing another sonic orifice to eliminate undesired larger particles before the seeding is fed into the cooling air supply. The final particle diameter is in the order of 800 nm. This seeding method was found to keep window contamination to a minimum. Laser illumination is provided by a standard, frequency-doubled, dual cavity Nd:YAG laser with 50 mJ pulse energy at 532 nm (green) and maximum repetition rate of 15 Hz (Quantel CFR Brio 50). The light is guided via an articulated mirror arm to the light sheet optics (pair of cylindrical lenses, pair of collimating spherical lenses). From there two redirection mirrors introduce the parallel light sheet radially through the top window into the transparent model of the cooling channel. The low divergence parallel light sheet matches the prismatic model geometry in order to avoid laser flare from the inclined divider wall (**Fig. 6**). The thickness of the light sheet is matched along its radial path to decreasing circumferential velocity with the radius. Thus, at the outer radius of 520 mm with higher channel offset between both laser pulses, the light sheet thickness started with 1.25 mm and reduces down to 0.8 mm at the inner radius of 280 mm to minimize the loss of particle pairs within the light sheet between the two successive recordings.. The light sheet position is adjusted in height by a traversable mirror. On the recording side, two thermo-electrically cooled, interline-transfer CCD cameras (pco.2000, 2048×2048 pixel, pixel size 7.4×7.4 μm², 14 bit, 7 fps, 4 GB camRAM) with a macro lens (Zeiss 85 mm, f# 1.4) are used. Band pass filters with centre frequency of 532 nm and 5 nm bandwidth (FWHM) were placed in front of the lenses to reject most of the unwanted background light. Because of the stretched rectangular channel geometry of 228 x 40 mm² it is observed simultaneously by two cameras positioned side by side with rectangular view on the light sheet plane. With an overlap of 13%, the cameras each recorded a field of 112 x 40 mm² at a magnification factor of 16.5 pixel/mm. Hence, the region of interest on the sensor could be reduced to 2048×640 pixel. Both cameras are adjusted in height by traverse units keeping the distance fixed for different light sheet planes and therefore the magnification factor constant. The reduced region of interest increased the number of images storable in the available camRAM of 4 GB up to 915 or 922 PIV double-images as well as it increased camera's frame rate with beneficial effect on the overall system frame rate.

Synchronization was provided by a newly developed FPGA sequencer which dynamically monitors the circumferential velocity to accurately trigger the cameras, laser flash lamp and Q-switch [2]. The PIV measuring equipment is arranged outside the rotating components, that is, in a lab-stationary frame. The desired measuring plane has to be synchronized exactly to a specified circumferential position of the test model, rotating with a varying circumferential velocity of about 680 rpm for Ro = 0.1. At every desired circumferential position (resolved continuously with an accuracy of 0.025 deg) the exact trigger times for the flash lamps, Q-switches and cameras can be extremely precisely estimated. TTL control signals are emitted over a high speed digital I/O module (NI-9401) [30]. Depending on the rotation number the pulse delay between the laser pulses varied between 12 and 8 µs (Ro = 0.1 and 0.0).

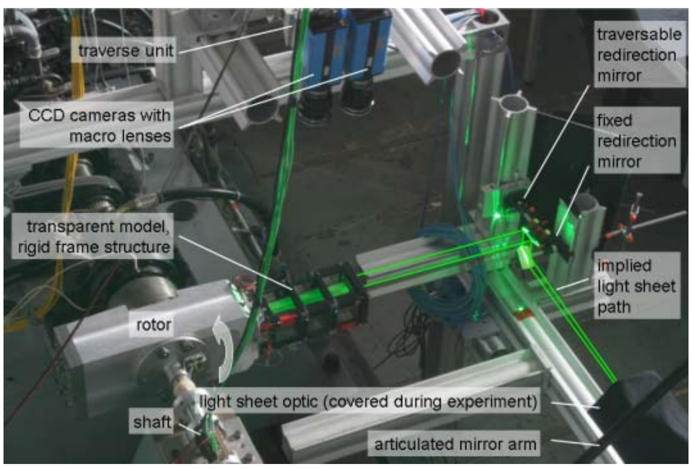

Fig. 5 Optical set-up of PIV at the rotating test rig for axial flow investigation, light sheet visible in second passage by tracer particles, Ro = 0.0

For the investigation of axial flow of the two-pass system, two camera positions in tangential direction to the model were chosen. **Fig. 5** shows the optical set-up of the PIV system on the rotating test rig for axial flow investigations in the second pass at horizontal circumferential position. The light sheet is inserted radially from the right side through the model's top window. The pair of two parallel cameras is positioned *above* the horizontal channel observing from camera position A through channels upper side (**Fig. 6**). In this configuration, the cooling channel is moving towards the cameras for the measurement of the second pass flow. The optical set-up of the PIV system was shifted to the left side regarding the rotation axis for the first pass investigation. Though the camera pair is as well positioned *above* the horizontal channel, the observation direction for this set-up was through model's lower side at the opposite horizontal circumferential position (φ +180°). Thus, for the measurement planes in the first pass the model is moving away from the camera between the two laser flashes.

Fig. 6 illustrates the discussed measuring planes for the axial flow field investigation in both passes. Camera view A with inclination angle of 8 degrees was used for all measurement planes in the second passage. Camera pair and light sheet were adjusted to mid plane and traversed synchronously in height to upper or lower side plane at ±65% of dimension. For first passage measurement planes camera views B and C with respective inclination angles of 30 and 42.5 degrees had to be used, because observation from *above* was blocked by the rigid frame structure required for structural support at higher rotation numbers. The disadvantage of this observation configuration is the optical blockage on both border sides due to back taper and especially on the ligament side with additional non-transparent silicon seam (accentuated by dashed areas). Nevertheless, with the approach from below at least the lower and mid plane could be examined in profitable extension. The upper side plane of the first passage was not measured because of poor remaining evaluable region (dashed line).

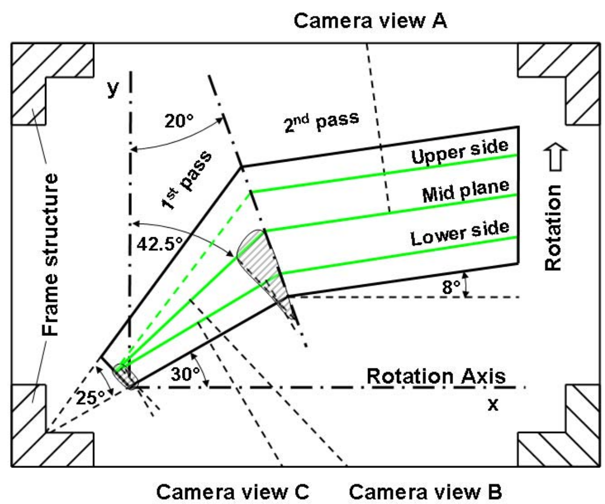

Fig. 6 PIV measurement planes for axial flow v_{xz} in two pass system outlining the viewing geometries

The rotation of the cooling channel with respect to the fixed camera introduces apparent velocity components, even though the angle of view is perpendicular on the light sheet. This systematic error is a result of the induced out-of-plane component which is of similar magnitude as the circumferential velocity. With a focal length of 85 mm, a distance from camera chip to light sheet of 720 mm and imaged width of 112 mm the half angle of view is AOV≈4.5°. Additional the cameras are inclined (8, 30 or 42.5 degrees) but rotational movement is straight vertical. The out-of-plane offset is subject to rotation angle φ, therefore to pulse distance as well as to local circumferential velocity as function of radius; thus the perspective projection is a function of radius. The minimum perspective projection occurs at camera's optical axis and increases to outer regions with maximum of AOV ≈ 4.5°. Due to the additional inclination angle the perspective projection shows a constant off-set (**Fig. 7**).

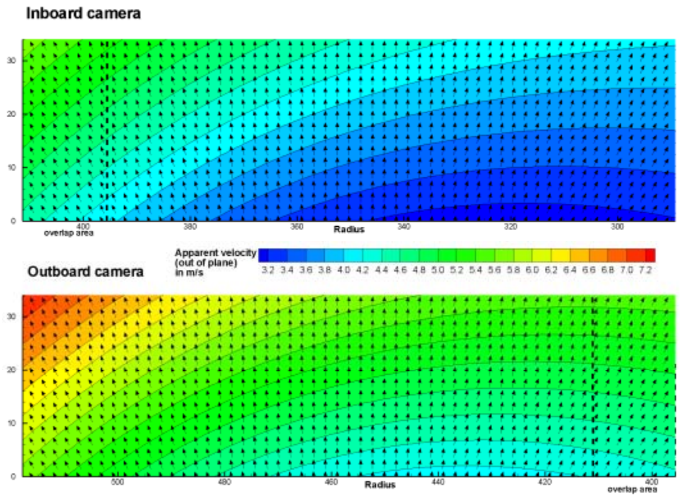

Fig. 7 Combined velocity vector map of perspective error as function of radius and inclination angle of 8°, in- and outboard camera at middle plane in the second passage

Fig. 7 clarifies the resulting velocity vector map based on perspective error is growing with radius from right to left hand side in magnitude within the second passage. Both vector maps exhibit a “tunnel effect” but with significantly shifted center due to inclination angle. In the area of overlap (r = 395 ... 411) the radial components are opposite due to the difference in viewing angle; they prevent a smooth transition between the two velocity maps.

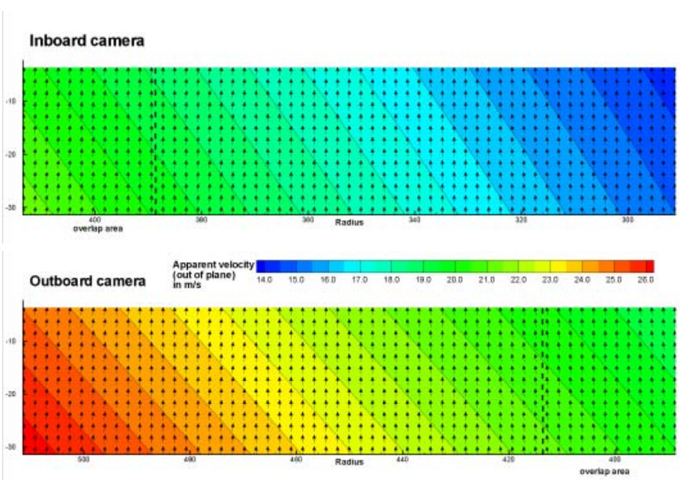

Fig. 8 Combined velocity vector map of perspective error as function of radius and inclination angle of 42.5°, in- and outboard camera at middle plane in the first passage

Fig. 8 shows the velocity vector map of systematically perspective error for the first passage. The previously mentioned “tunnel effect” is significantly reduced and in comparison the vectors are point to the center because the rotor is moving away for this setup. The perspective error increases with radius from right to left hand side in magnitude again, but at a significant higher level of 26.0 m/s compared to 6.6 m/s in maximum for the second passage. The orientation of all vectors is more or less straight vertical. The inclination angle becomes the major effect and reaches the magnitude of examined flow field in the bend region.

The accuracy of the PIV measurements technique itself for the non-rotating model is better than 1% of full scale. This is confirmed both by means of reference measurements performed on a calibration nozzle as well as by comparison with L2F velocimetry measurements in the same model [19]. Following the approach made by Westerweel [31] the estimated measurement error made at optimal PIV measurements conditions is on the order of 0.1 pixels (here 0.8 m/s). To obtain velocity maps the collected image pairs were processed with the PIV software PIVview2C which implants a state-of-the-art multi-grid interrogation algorithm with an initial sampling window of 96×96 pixel and final window size of 24×24 pixel on a sampling grid of 12×12 pixel. Each velocity vector represents the averaged flow within an area of 1.46×1.46 mm² at a spatial resolution of 0.73 mm grid distance. The velocity vector maps are averaged out of 922 double-images for first passage and 915 for second passage flow field images. The above mentioned perspective error is finally subtracted from the average velocity vector map. For better visualization the PIV maps presented in this paper are plotted with streamlines.

THEORETICAL BACKGROUND

THE MAIN FLOW PHYSICAL MECHANISMS

The flow inside the two-pass system is influenced by four primary factors:

i. bend induced Dean vortices in the 180 degree turn,
ii. separation along the dividing wall in the second passage,
iii. vortices induced by the ribs in both passes and
iv. Coriolis vortices induced by rotation in both passes.

All flow phenomena and vortices interact with each other resulting in a complex 3D flow, especially in the second pass.

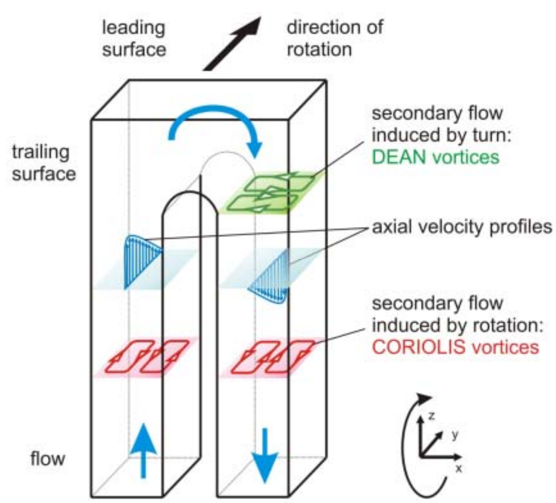

Fig. 9 Bend induced counter-rotating Dean vortices and rotation induced counter-rotating Coriolis vortices in both passes (sketched here non interacting)

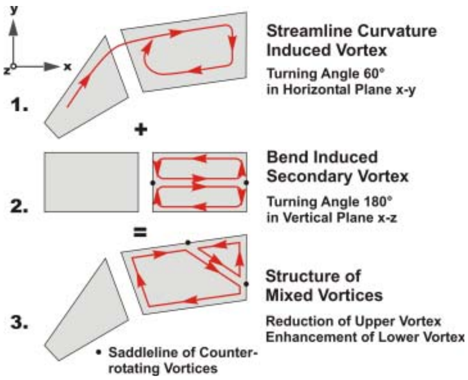

Fig. 10 Superposition of bend induced vortices in the smooth second passage

The effect of the bend on the flow

The flow in the smooth channel is influenced by two factors: As a consequence of the engine-similar geometry, the main flow at the bend impinges onto the upper side of the second passage and further downstream to the rear duct wall (**Fig. 10.1)**. It induces a roll-up of the flow to form a strong vortex ("impingement effect"). Within the bend, centrifugal forces cause a secondary flow development of two counter-rotating vortices as sketched in **Fig. 10.2** ("Dean effect") [32]. By superposition of both phenomena the flow situation is derived for the smooth rear pass. The upper vortex is clearly weakened as the lower one is enhanced, **Fig. 10.3**. With interaction of these vortices in this real configuration, the saddle points of the vortices are moved to the new positions marked by black dots.

The effect of rotation on the flow

Rotation induces Coriolis vortices in both passages. Depending on the flow direction radially outward or inward, the rotation sense of the vortex pair is changed as sketched in **Fig. 9** by the red vortex pair. By superposition of the Dean vortices with the Coriolis vortices, the flow situation in the (smooth) rear pass is derived. The upper vortex is clearly weakened as the lower one is enhanced, which was also observed in earlier measurements [1],[22].

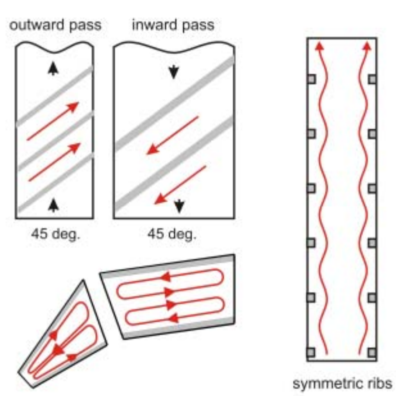

Fig. 11 Rib induced counter-rotating vortex pair in both passes

The effect of wall ribs on the flow

In order to enhance heat transfer the channel is equipped with wall turbulators in form of square sectioned ribs. With inclined ribs in the same orientation on both opposite walls, two symmetric vortices are generated within both passages, as sketched in **Fig. 11,** compare to [1] for stationary PIV results.

RESULTS

PIV FLOW MEASUREMENTS

In the following, experimental results from PIV are presented in the form of isolines of the axial in-plane velocity:

$$v_{xy} = \sqrt{\overline{v_x}^2 + \overline{v_y}^2}\,,$$

where $\overline{v_x}$, $\overline{v_y}$ are velocity components averaged out of 922 instantaneous PIV recordings (first pass) and 915 recordings (second pass), respectively. The magnitude of the velocity is depicted by color contours. The orientation of the flow field is implied by streamlines generated within Tecplot®. Three cuts were presented to analyze the axial flow: +65, 0 and -65% of the half duct height. The longitudinal cut position of ±65% was the closest wall distance avoiding laser flare from the ribs with respect to the laser light sheet thickness of 1.25 mm at the outer radius together with maximum rotational offset. The positions of the longitudinal measuring cuts are as well given in **Fig. 6**.

The investigation of the axial flow

Smooth channel, no rotation

Fig. 12 shows the measured axial velocity distribution in the smooth channel configuration at lower side (a), mid plane (b) and upper side (c) in the first and second pass for Re = 50,000 and non-rotating (Ro = 0.0). For the upper side plane the flow field for the first passage is missing due to insufficient optical access as discussed before. Each longitudinal cut is combined from two separate but simultaneous fields of view. The obvious trisection is caused by optical blockage from the surrounding rigid frame (see **Fig. 5**). Unfortunately about 40% of the quite interesting region around the bend is lost because of occlusion by the frame structure. Due to the parallel light sheet geometry the intersection between inlet and outlet pass in thickness of the separation wall could not be illuminated. Nevertheless, the remaining optically accessible region gives an excellent insight to axial flow structure and a promising validation data set for numerical prediction like given in [26],[33].

In the inlet passage the flow for both cuts do not exhibit any distinctive features $\boxed{1}$ except the onset of flow turning $\boxed{2}$ near the bend. Directly behind the bend a separation bubble with reverse flow is visible $\boxed{3}$. Beneath the separation bubble the flow is strongly accelerated impinging the rear wall $\boxed{4}$. The separation bubble shows extremely three-dimensional behaviour; its size and downstream extension increases from the lower side towards the upper side $\boxed{5}$. Shape and extension of the measured separation bubble is well predicted by the DLR numerical flow solver TRACE already presented in [33].

Smooth channel, with rotation

Fig. 13 shows the measured axial velocity distribution in the smooth channel configuration with rotation (Ro = 0.1) at lower side (a), mid plane (b) and upper side (c) in the first and second pass for Re = 50,000. The flow in the inlet pass is apparently accelerated somewhat over the non-rotating values $\boxed{1}$ for yet unknown reasons but in accordance with CFD results.

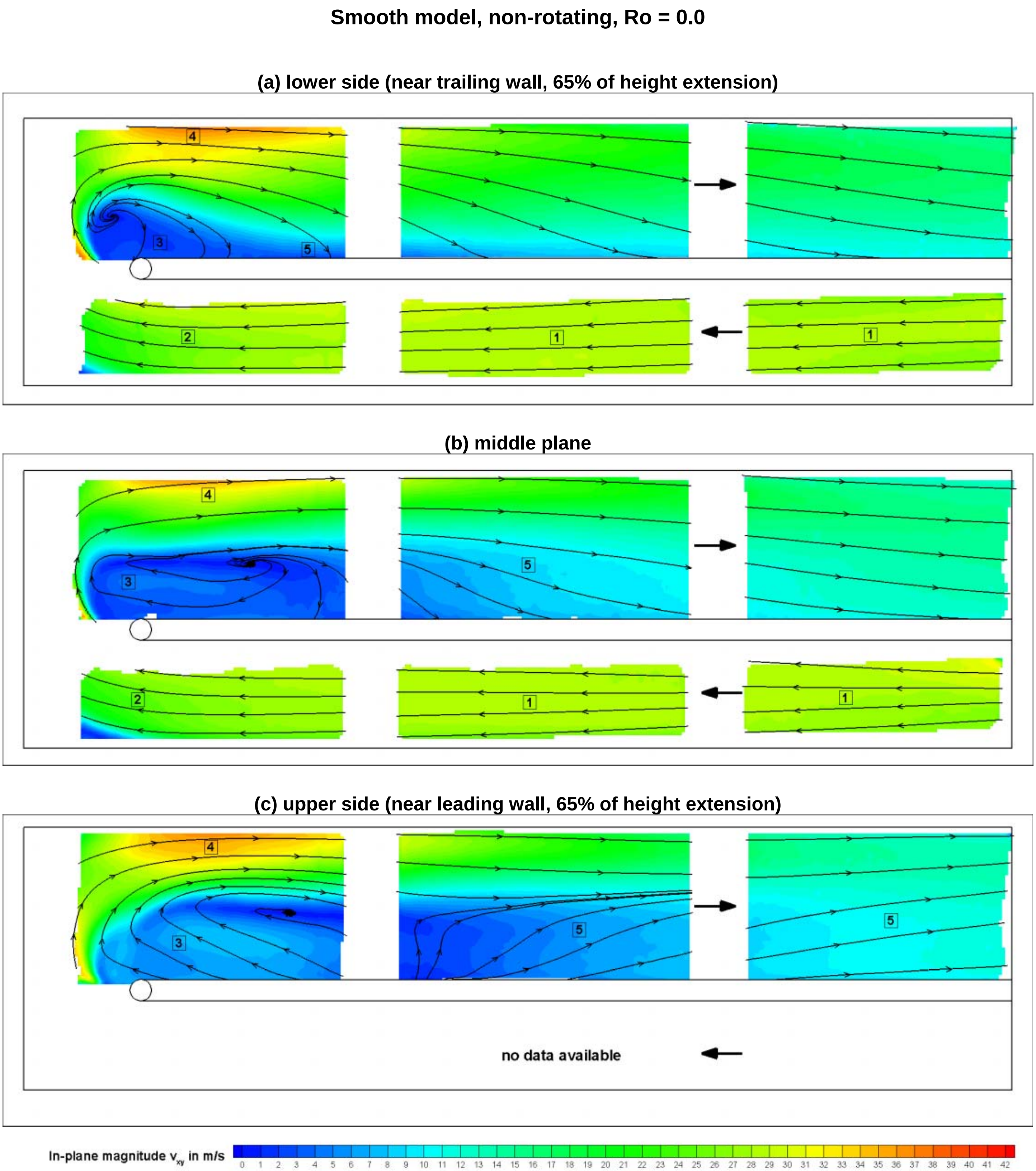

Fig. 12 Axial in-plane flow velocity distribution, here smooth model, Re = 50,000, Ro = 0.0 (non-rotating), streamlines for visualisation generated within Tecplot®

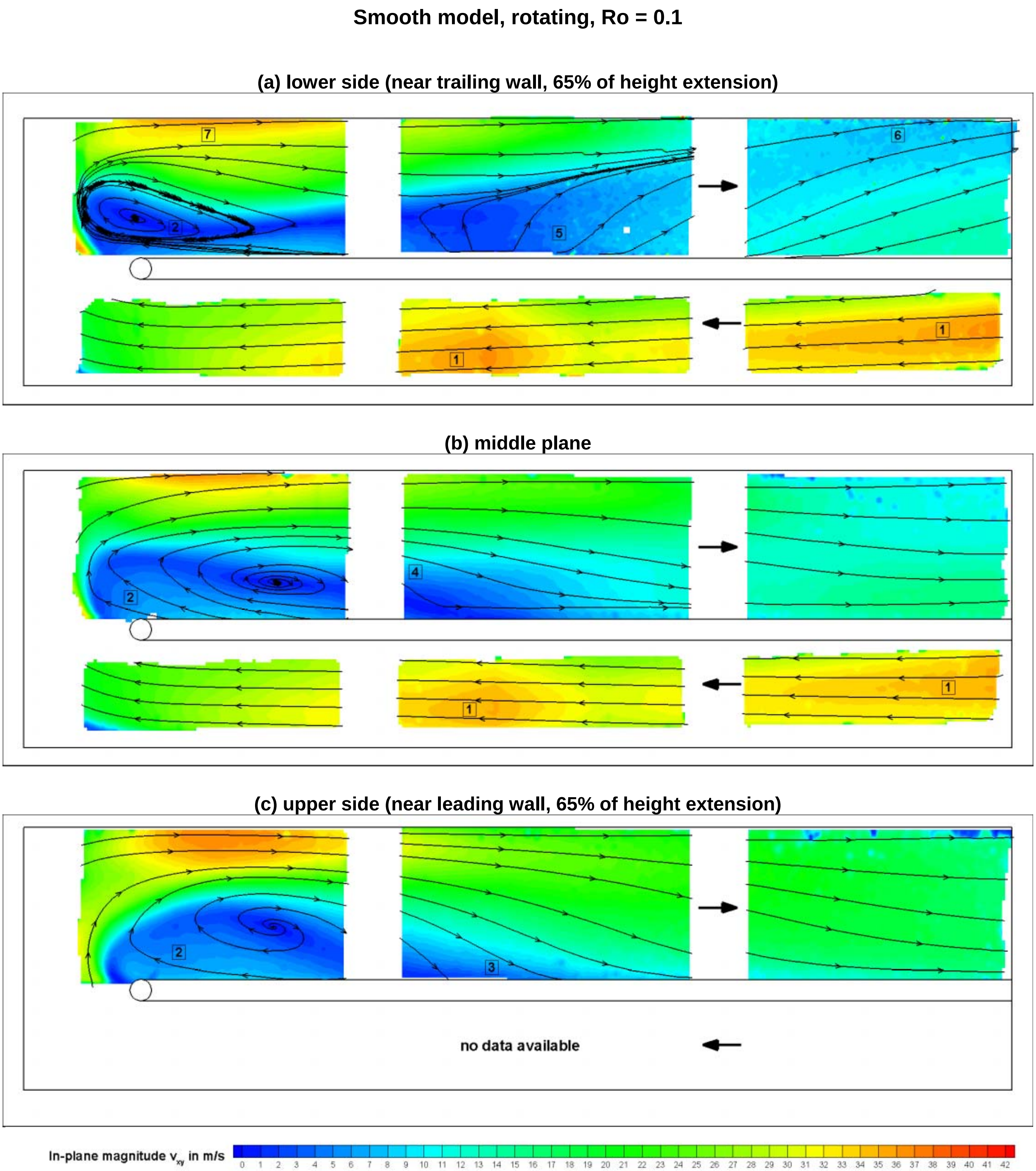

Fig. 13 Axial in-plane flow velocity distribution, here <u>smooth</u> model, Re = 50,000, Ro = 0.1 (<u>rotating</u>), streamlines for visualisation generated within Tecplot®

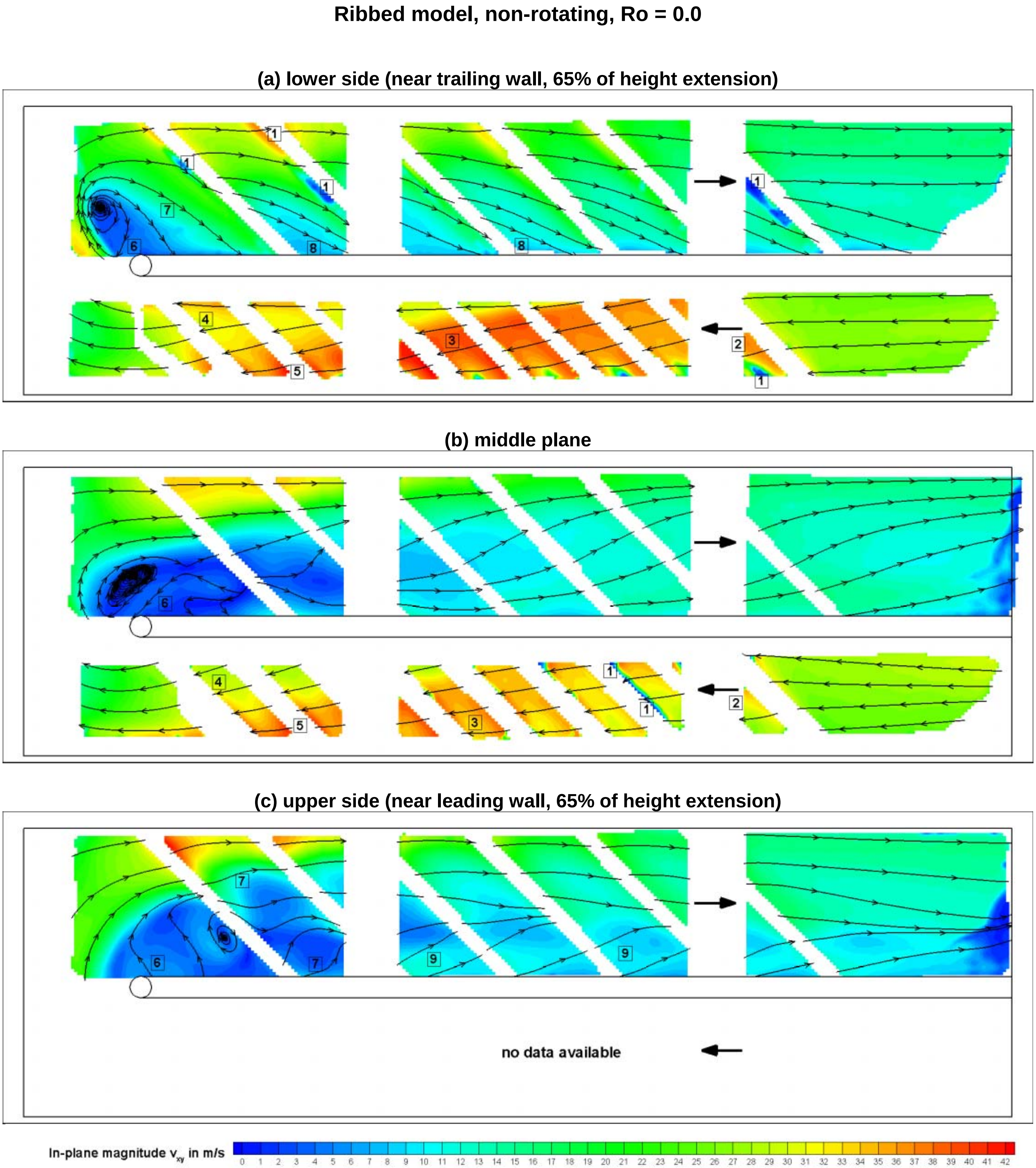

Fig. 14 Axial in-plane flow velocity distribution, here ribbed model, Re = 50,000, Ro = 0.0 (non-rotating), streamlines for visualisation generated within Tecplot®

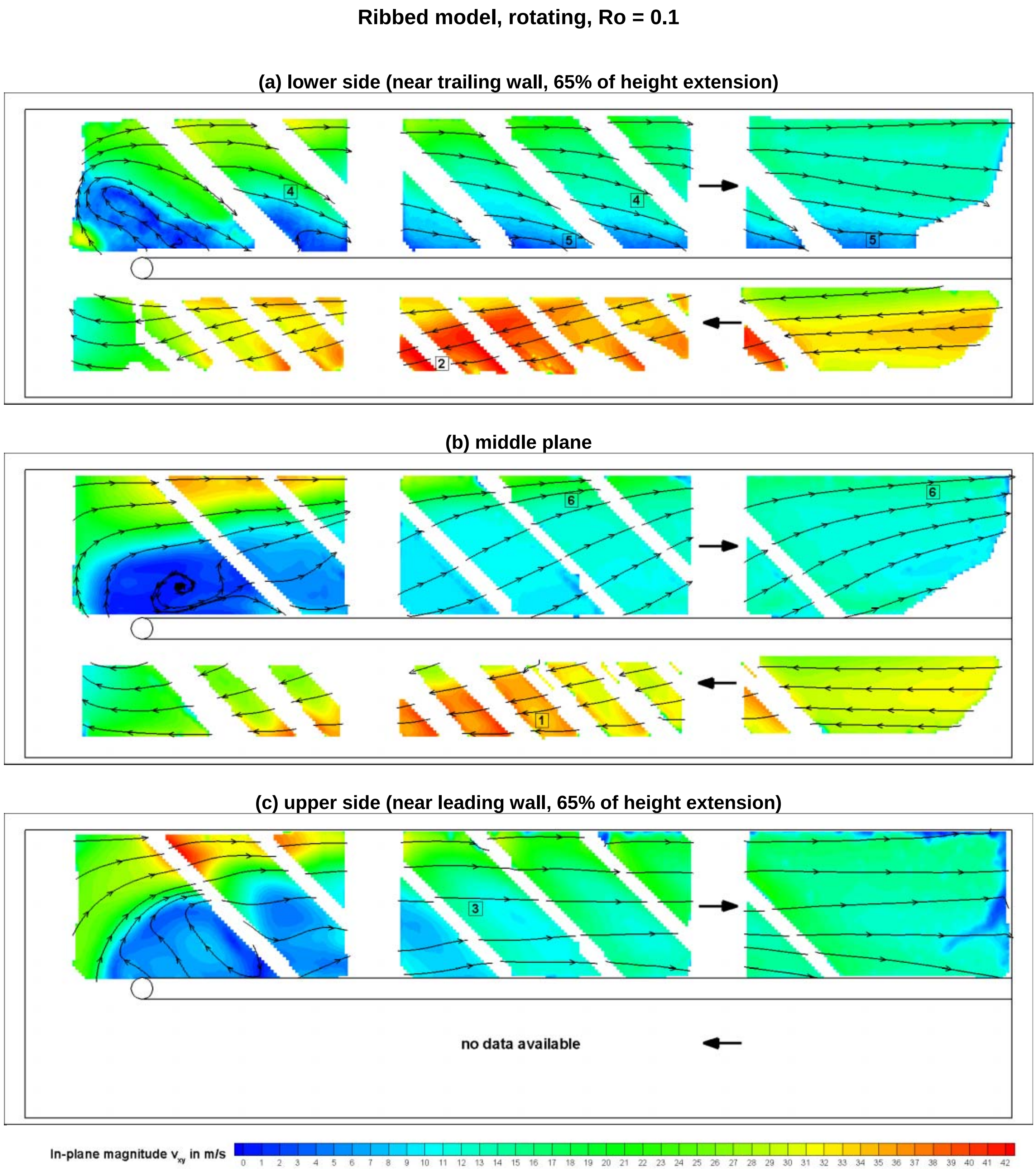

Fig. 15 Axial in-plane flow velocity distribution, here ribbed model, Re = 50,000, Ro = 0.1 (rotating), streamlines for visualisation generated within Tecplot®

The separation bubble behind the bend is strongly affected by rotational forces $\boxed{2}$. At the upper side, the extension of the separation bubble is reduced to only half the channel length against the non-rotating configuration $\boxed{3}$. In the middle plane the separation is weakened $\boxed{4}$. At the lower side, the separation zone shows a region of low local velocity and therefore of low kinetic energy which is spreading from the divider wall $\boxed{5}$ to the opposite rear wall $\boxed{6}$ as a consequence of the different rotational vortex regime. In general, the impingement of flow to the rear wall is strengthened downstream of the bend resulting in higher flow velocities $\boxed{7}$.

Ribbed channel, no rotation

In **Fig. 14** the measured axial velocity distribution in the ribbed channel configuration at lower side (a), middle plane (b) and upper side (c) in the first and second pass for Re = 50,000 and non-rotating (Ro = 0.0). The non-transparent ribs partially occlude the field of view, especially in the first passage in the vicinity of the sharp corner at the leading edge. Small and discrete patches of high velocity gradients in the direct vicinity of the ribs $\boxed{1}$ are PIV processing artefacts due to mismatched correlation or filter setting and should be neglected. At the inlet passage the flow acceleration is clearly visible behind the first rib $\boxed{2}$ as well as a slight redirection in the direction of leading edge $\boxed{3}$ to provide better heat transfer at the stagnation point where the highest heat input is present. Within the first duct, no fully developed flow structure can be observed $\boxed{4}$; the trend of flow acceleration near leading edge is clearly visible $\boxed{5}$.

After passing the divider wall the separation bubble $\boxed{6}$ with strong reverse flow components also forms but is reduced in extension in comparison to the smooth channel (**Fig. 12**). At the lower side the bubble does not seem to enter the ribbed channel part, whereas at the upper side the separation bubble immediately spreads across the whole upper wall $\boxed{7}$. The flow field is asymmetric and the vectors at the lower side are in direction of rib orientation $\boxed{8}$. The flow seems to flush into the gap between the ribs, whereas on the upper side this behaviour is significantly reduced and close to the divider wall the flow almost seems to trip over the ribs $\boxed{9}$.

Ribbed channel, with rotation

In **Fig. 15** the previously discussed ribbed configuration is shown for all three cuts in the first and second passage for Re = 50,000 and rotation (Ro = 0.1). The inlet passage was nearly unaffected by rotation $\boxed{1}$ and looks similar to **Fig. 14**. However, as found in the smooth channel configuration, higher velocities were induced near the lower wall $\boxed{2}$.

Downstream of the bend the separation zone on the upper side was reduced during rotation by half in size and extension $\boxed{3}$ quite similar to the smooth model behaviour (**Fig. 13**). Streamlines are not affected by the inclination of ribs. At the lower side the flow follows the rib orientation $\boxed{4}$ and the separation bubble at divider wall increases in length $\boxed{5}$ in comparison to the smooth model (**Fig. 13**). The middle plane shows the rib induced adverse flow directed toward the back wall $\boxed{6}$ as sketched in the cross-section in **Fig. 11**. In general, rotational effects are weak while rib effects dominate.

SUMMARY

In continuation of previous successful PIV measurements obtained of the secondary flow within two-pass cooling channels using a new sequencer technique the axial flow field was investigated extensively. This paper described the experimental investigation of a two-pass cooling system as part of a multi-pass turbine blade cooling system with and without ribbed walls with the additional impact of rotation. A complex flow situation is present:

i. rib induced vortices were generated in both passes and were found to dominate all other effects at the chosen operating conditions,
ii. bend induced vortices appear in the beginning of the second passage,
iii. rotation induced Coriolis vortices are present mainly in the second passage at Ro = 0.1; they do not appear in classical shape but they have a strong effect to the development of the separation bubble and of the flow.

The presented experiments are part of a long term investigation in cooperation with the Stuttgart University where heat transfer is investigated in detail. The flow investigations have started with the basic geometry of a square-sectioned duct, presented by Elfert [22]. Instead of the simple basic geometry, the additional effect of the engine similar geometry is presented in this paper. The PIV data from this research work will be used in-house for further flow analysis and, additionally, for validation and development of CFD at DLR Cologne [26],[33]. Both, measurements and simulation, contribute to an improved understanding of the complex flow phenomena present in such cooling systems.

ACKNOWLEDGMENTS

The project was conducted as part of the joint research programme **COOREFF-T** in the frame of AG Turbo. The work was supported by the Bundesministerium für Wirtschaft und Technologie (BMWi) as per resolution of the German Federal Parliament under the grant number **0327713S.** The authors gratefully acknowledge AG Turbo and MAN-Turbo, MTU, Rolls Royce Germany and Siemens for their support and permission to publish this paper. The engaged participation of C. Willert, E. Nicke, S. Grund and M. McNiff from DLR in this project is also gratefully acknowledged.

REFERENCES

[1] Elfert, M., Jarius, M., Weigand, B.: Detailed Flow Investigation using PIV in a Typical Turbine Cooling Geometry with Ribbed Walls, Proceedings of ASME Turbo Expo, June 14-17, 2004, Vienna, Austria, Paper GT-2004-53566.

[2] Elfert, M., Schroll, M., Förster, W.: PIV-Measurement of secondary flow in a rotating two-pass cooling system with an improved sequencer technique, Proceedings of ASME Turbo Expo, June 14-18, 2010, Glasgow, UK, Paper GT-2010-23510.

[3] Lezius, D.K. and Johnston, J.P.: Roll-Cell Instabilities in Rotating Laminar and Turbulent Channel Flows, Journal of Fluid Mechanics, 77, p.153-175, 1976.

[4] Elfert, M.: The Effect of Rotation and Buoyancy on Flow Development in a Rotating Circular Coolant Channel, 2nd Int. Symposium on Engineering Turbulence Modelling and

Measurements, May 31-June 2, 1993, Florence, Italy, p.815-824.
[5] Elfert, M., Hoevel, H., Towfighi, K.: The Influence of Rotation and Buoyancy on Radially Inward and Outward Directed Flow in a Rotating Circular Coolant Channel, Proc. 20th ICAS Conference, 1996 Sorrento, Italy, 2490-2500.
[6] Rathjen, L., Hennecke, D.K., Elfert, M., Bock, S., Henrich, E.: Investigation of Fluid Flow, Heat Transfer and Pressure loss in a Rotating Multi-Pass Coolant Channel with an Engine Near Geometry, ISABE-Conference, Florence, 1999, ISABE- IS-216.
[7] Tse, D.G.N., McGrath, D.B.: A Combined Experimental/Computational Study of Flow in Turbine Blade Cooling Passage, Part I: Experimental Study, ASME Paper No. 95-GT-355, 1995.
[8] Tse, D.G.N., Steuber, G.D.: Flow in a Rotating Square Serpentine Coolant Passage with Skewed Trips, ASME Paper No. 97-GT-529, 1997.
[9] Cheah, S.C., Iacovides,, H., Jackson, D.C., Ji, H., Launder, B.E.: LDA Investigation of the Flow Development through Rotating U-Ducts, ASME J. Turbomachinery 118: 590-595, 1996.
[10] Bons, J.P., Kerrebrock, J.L.: Complementary velocity and heat transfer measurements in a rotating cooling passage with smooth walls. ASME, J. of Turbomachinery, 121, p. 651–662, 1999.
[11] Bonhoff, B., Parneix, S., Leusch, J., Johnson, B. V., Schabacker, J., Bölcs, A.: Experimental and numerical study of developed flow and heat transfer in coolant channels with 45 degree ribs, Int. J. Heat and Fluid Flow, 20, Issue 3, June, p. 311-319, 1999.
[12] Chanteloup, D., Juaneda, Y., Bölcs, A.: Combined 3D Flow and Heat Transfer Measurements in a 2-Pass Internal Coolant Passage of Gas Turbine Airfoils, ASME, Paper GT-2002-30214
[13] Son, S.Y., Kihm, K.D., Han, J.C.: PIV Flow Measurements for Heat Transfer Characterization in Two-Pass Square Channels with Smooth and 90-degree Ribbed Walls, Int. J. of Heat and Mass Transfer, 45, no. 24, p. 4809-4822, 2002.
[14] Liou, T.M., Chen, C.C.: LDV Study of Developing Flows through a Smooth Duct with a 180 Deg Straight-Corner Turn, ASME J. of Turbomachinery, 121, p. 167-174, 1999.
[15] Liou, T.M., Chen, M.Y., Tsai, M.H.: Fluid Flow and Heat Transfer in a Rotating Two-Pass Square Duct with In-Line 90° Ribs, ASME Paper GT 2001-0185.
[16] Liou, T.M., Chen, M.Y., Wang, Y.M.: Heat Transfer, Fluid Flow, and Pressure Measurements inside a Rotating Duct with Detached 90° Ribs," ASME Paper GT 2002-30201.
[17] Liou, T. M., Dai, G. Y.: Pressure and Flow Characteristics in a Rotating Two-Pass Square Duct with 45 Deg Angled Ribs, ASME Paper No. GT 2003-38346.
[18] Liou, T.M., Hwang, Y.S., Li, Y.C.: Flow Field and Pressure Measurements in a Rotating Two-Pass Duct with Staggered Rounded Ribs Skewed 45° to the Flow," ASME Paper GT 2004-53173.
[19] Elfert, M., Jarius, M. P.: Steady Fluid Flow Investigation using L2F and PIV in a Multi-Pass Coolant Channel. 9th Int. Symp. on Transport Phenomena and Dynamics of Rotating Machinery (ISROMAC-9), Honolulu, Hawaii, Feb.10-14, 2002.
[20] Jarius, M. P., Elfert, M.: Flow Investigation in a Two-Pass Coolant Channel with/without Ribbed Walls. 16th Int. Symp. on Air Breathing Engines, Aug. 31- Sept. 5, 2003, Cleveland, Ohio, USA, Paper ISABE-2003-1155.
[21] Elfert, M., Jarius, M.: Detailed Flow Investigation in a Ribbed Turbine Blade Two-pass Cooling System, 17th International Symposium on Air Breathing Engines (ISOABE), September 4-9, 2005, Munich, Germany.
[22] Elfert, M., Voges, M., Klinner, J.: Detailed Flow Investigation Using PIV in a Rotating Square-sectioned Two-pass Cooling System With Ribbed Walls, ASME Turbo Expo, June 9-13, 2008, Berlin, Germany, Paper GT-2008-51183.
[23] Gallo, M. and Astarita, T.: PIV measurements in a rotating channel, 7th International Symposium on Particle Image Velocimetry, Faculty of Engineering, University "La Sapienza", Rome, 11-14 Sept., 2007, Italy.
[24] Schubert, S., Neumann, S.O., Jarius, M.P., Elfert, M., Weigand, B.: Investigation of Flow Phenomena and Heat Transfer Performance of a Ribbed Two-pass Cooling Channel with Turbine Typical Cross Sections. 16th Int. Symp. on Air Breathing Engines, Aug. 31- Sept. 5, 2003, Cleveland, Ohio, USA, Paper ISABE-2003-1156.
[25] Schüler, M., Neumann, S.O., Weigand, B.: Pressure Loss and Heat Transfer in a 180 deg Bend of a Ribbed Two-pass Internal Cooling Channel with Engine-similar Cross-section, Pt.2: Numerical Investigations, Proc. 8th European Turbomachinery Conference, March 23-27, 2009, Graz, Austria.
[26] Schüler, M., Dreher, H.-M. , Neumann, S. O., Weigand, B., Elfert, M.: Numerical Predictions of the Effect of Rotation on Fluid Flow and Heat Transfer in an Engine-Similar Two-Pass Internal Cooling Channel with Smooth and Ribbed Walls, ASME Turbo Expo, June 14-18, 2010, Glasgow, UK, Paper 2010-22870.
[27] Iacovides, H., Launder, B. E.: Internal blade cooling: the Cinderella of computational and experimental fluid dynamics research in gas turbines, Proceedings of the I MECH E Part A Journal of Power and Energy, Volume 221, Number 3, 2007, pp. 265-290(26).
[28] Adrian, R.J.: Particle-Imaging Techniques for Experimental Fluid Mechanics, Annual Review of Fluid Mechanics, vol. 23, 1991.
[29] Raffel, M., Willert, C., Wereley, S., Kompenhans, J.: Particle Image Velocimetry – A practical guide (2nd Edition). Springer Berlin Heidelberg, 448 pages (ISBN: 978-3-540-72307-3), 2007.
[30] Förster, W., Klinner, J., Voges, M., Willert, C., Elfert, M.: Phasensynchroner FPGA-Pulsgenerator für Particle-Image-Velocimetry Messungen an rotierenden Maschinen mit stark schwankender Drehzahl. In: Virtuelle Instrumente in der Praxis, pp. 90-94. Hüthig Verlag VIP 2009, Oct 7, 2009, Munich, Germany, ISBN 978-3-7785-4057-2.
[31] Westerweel J.: Theoretical analysis of the measurement precision in particle image velocimetry. Exp Fluids 29: Suppl. S3-S12, 2002.
[32] Dean, W.R.: The stream-line motion of fluid in a curved pipe. Philosophical Magazine, S.7, 1928, Vol. 4, No. 20, 208 – 223.
[33] Schüler, M., Dreher, H.-M. , Neumann, S. O., Weigand, B., Elfert, M.: Numerical Predictions of Fluid Flow and Heat Transfer in a Rotating Engine-Similar Two-Pass Internal Cooling Channel With Smooth and Ribbed Walls, 13th Int. Symposium on Transport Phenomena and Dynamics of Rotating Machinery (ISROMAC), Honolulu, Hawaii, April 4-9, 2010, Paper ISROMAC13-2010-20104.

